(Pr, Ho)-Fe-B magnets for low-temperature applications

Cite as: AIP Advances **9**, 125025 (2019); https://doi.org/10.1063/1.5129896
Submitted: 03 October 2019 . Accepted: 02 November 2019 . Published Online: 19 December 2019

Nataliya B. Kolchugina, Katerina Skotnicova, Aleksander A. Lukin, Gennadii S. Burkhanov, Ondrej Zivotsky, Miroslav Kursa, Nikolay A. Dormidontov, Pavel A. Prokofev, Yuri S. Koshkidko, Tomas Cegan, Tatiana P. Kaminskaya, and Boris A. Ginzburg

(Pr, Ho)-Fe-B magnets for low-temperature applications

Cite as: AIP Advances 9, 125025 (2019); doi: 10.1063/1.5129896
Presented: 5 November 2019 • Submitted: 3 October 2019 •
Accepted: 2 November 2019 • Published Online: 19 December 2019

Nataliya B. Kolchugina,[1,a)] Katerina Skotnicova,[2] Aleksander A. Lukin,[3] Gennadii S. Burkhanov,[1] Ondrej Zivotsky,[4] Miroslav Kursa,[2] Nikolay A. Dormidontov,[1] Pavel A. Prokofev,[3] Yuri S. Koshkid'ko,[1,5] Tomas Cegan,[2] Tatiana P. Kaminskaya,[6] and Boris A. Ginzburg[6]

AFFILIATIONS

[1]Baikov Institute of Metallurgy and Materials Science, Russian Academy of Sciences, 119 334 Moscow, Russian Federation
[2]VSB-Technical University of Ostrava, FMST, Regional Materials Science and Technology Centre, 708 00 Ostrava, Czech Republic
[3]JSC SPETSMAGNIT, 127 238 Moscow, Russian Federation
[4]VSB-Technical University of Ostrava, Department of Physics, 708 00 Ostrava, Czech Republic
[5]Institute of Low Temperature and Structure Research, Polish Academy of Sciences, 50 422 Wroclaw, Poland
[6]Physical Department, Moscow State University, 119 991 Moscow, Russian Federation

Note: This paper was presented at the 64th Annual Conference on Magnetism and Magnetic Materials.
[a)]**Corresponding author. Email:** natalik014@yandex.ru

ABSTRACT

We have investigated the effect of HoH_2 hydride addition on the hysteresis loop parameters of sintered Pr-Fe-Ti-Al-Cu-B magnets. The magnets were prepared by traditional powder metallurgy technology, and 3 wt.% HoH_2 was added to the powder at the fine-milling stage. The magnets exhibited a monotonic increase in all hysteretic parameters with decreasing temperature down to 4.2 K. The coercive force and maximum energy product at 295 K (4.2 K) were 1344 (5402) kA/m and 221 (336) kJ/m^3, respectively. The structure of the magnets was studied in detail by scanning electron microscopy and energy dispersive X-ray spectroscopy, which demonstrated the formation of the so-called "core-shell" structure, which is assumed to favor the marked improvement in the hysteretic properties of the samples analyzed. The surface domain structure was measured in the directions perpendicular and parallel to the magnet texture using magnetic force microscopy. The data obtained indicated fine labyrinth-like and strip domain patterns in the directions perpendicular and parallel to the magnet texture, with an average domain width of 1.2–1.8 μm.

I. INTRODUCTION

In recent years, permanent magnets based on (Pr, Nd)$_2$Fe$_{14}$B compounds have become potential candidates for applications at low temperatures (undulators, magnetic bearings, wigglers, etc.).[1–3] Nd$_2$Fe$_{14}$B-based magnets with a high remanence cannot be employed for the construction of undulators because of their weak coercivity at room temperature (RT). During cooling to 135 K, magnets exhibit a high resistance to demagnetization and a marked increase in their remanence and coercivity due to spin reorientation. At 135 K, the easy-axis magnetic anisotropy changes to easy-axis cone anisotropy and the spin-reorientation transition (SRT) takes place. The tilting angle increases with decreasing temperature and, as a result, the remanence drops below values corresponding to RT. Thus, the natural low-temperature-induced improvement in hysteretic properties cannot be used adequately, and, therefore, most Nd$_2$Fe$_{14}$B-based magnets must operate in the temperature range 200–450 K.

Previously, Pr$_2$Fe$_{14}$B-based magnets were not applied in practice despite the fact that most of their magnetic parameters at RT are better than or comparable with those of Nd$_2$Fe$_{14}$B. For example, the anisotropy field of Pr$_2$Fe$_{14}$B (8.7 T) is higher than that of Nd$_2$Fe$_{14}$B (6.7 T),[4] indicating the possible higher intrinsic coercivity ($_jH_c$) of the first-mentioned alloy, while the Curie temperature and the

saturation magnetization (569 K and 1.56 T, respectively)[5,6] are only slightly lower than those of $Nd_2Fe_{14}B$ (586 K and 1.60 T). Moreover, the $Pr_2Fe_{14}B$-based magnets exhibit no SRT down to 4.2 K.[7,8] All these factors make Pr-Fe-B alloys attractive for wide temperature range applications. On the other hand, these alloys exhibit the worst temperature and time stability.[9]

The Pr-Fe-B alloys are more viscous than the Nd-Fe-B alloys. This fact determines the higher quenching rates and assumes the application of hydrogen decrepitation. However, it was shown in Reference 10 that the presence of hydrogen changes the anisotropic nature of $Pr_{15}Fe_{79}B_6$ hydrogenated powders from uniaxial to planar in the range 4250–4500 ppm H_2. Thus, if the hydrogenated $Pr_2Fe_{14}B$ powder is compacted in a magnetic field, no texturing along the easy-magnetization axis takes place, and the powder behaves similarly to an isotropic system at RT. In this case, the hysteretic parameters of the magnets decrease abruptly. The authors of Reference 10 suggest either dehydrogenating the powder before compacting or alloying the composition with dysprosium (Dy).

The considerable interest shown by researchers in reducing the usage of Dy in Nd-Fe-B-based magnets has stimulated interest in the application of Ho-containing compounds. In Reference 11, the coercivity of Dy-free magnets was investigated through intergranular addition of eutectic $Ho_{63.4}Fe_{36.6}$ powders. The coercivity enhancement was explained by microstructural observations and elemental distribution analysis. However, $Ho_2Fe_{14}B$ exhibits spin reorientation at 58 K,[12] which is shifted to 90 K as a result of hydrogen absorption with increasing H_2 content.

The aim of the present study was to investigate the effect of HoH_2 additions, which were subjected to fine milling together with the hydrogenated $PrFeBH_x$ alloy, on the texture formation and properties of permanent magnets over the wide temperature range 4.2–295 K.

II. EXPERIMENTAL

The alloy containing (wt.%) Pr-33, Ti-0.9, Al-0.3, Cu-0.15, B-1.3, Fe-balance was prepared by induction melting in an argon atmosphere and cast into a water-cooled copper mold. The alloy was subjected to hydrogen decrepitation using a bell-type furnace, whose chamber was preliminarily washed with nitrogen gas and flashed with hydrogen. The hydrogenation process was then performed during heating to 473 K for 1.5–2 h where it was held for 1 h. The furnace chamber was then washed with nitrogen gas, and the alloy was subjected to furnace cooling to RT. Powders of the $Pr_2Fe_{14}B$-based alloy and its mixture with 3 wt.% HoH_2 were prepared by milling in an isopropyl alcohol medium using a vibratory ball mill. Magnet blanks were prepared by compacting at a force of 300 kg/cm^2 using a hydraulic press with a loading rate no faster than 10 mm/s. A texturing magnetic field of 1.6 T was applied perpendicular to the pressing force direction. The blanks were dried and sintered at 1375 K for 1 h (single-cycle technological operation) and subjected to low-temperature treatment at 775 K for 1 h using vacuum resistance furnaces. The resulting sample is denoted as (Pr,Ho)-Fe-B or $(Pr,Ho)_2Fe_{14}B$ magnet in the following text.

The microstructure and chemical composition of the phases were studied by scanning electron microscopy (SEM) using a QUANTA 450 FEG equipped with an energy dispersive X-ray (EDX) APOLLO X analyzer. The phase composition of the magnets was investigated by X-ray diffraction (XRD) analysis using an Ultima IV (Rugaku, Japan) diffractometer equipped with a D/teX detector and Cu Kα radiation. XRD patterns were taken in a 2θ angular range of 3°–100° at a scanning step of 0.001°. The qualitative and quantitative analyses of diffractograms were performed using the simplified Rietveld method, PHAN, and PHAN% software.

Magnets were first magnetized in a pulse magnetic field up to 12 MA/m. Additionally, a MH-50 hysteresisgraph with a close magnetic circuit and a vibrating-sample magnetometer (VSM) were used for measurements of the magnetic characteristics in magnetic fields of up to 2 MA/m (2.5 T) and 7.2 MA/m (9 T), respectively. Hysteresisgraph measures bulk magnetic properties of prepared magnets (30 mm in diameter and 10 mm high) at RT, while only small piece of magnet (mass about 100 mg) is analyzed using the VSM in the temperature range 4.2–295 K. The domain structure of the samples was observed in directions perpendicular and parallel to the magnet texture by magnetic force microscopy (MFM) using Solver Pro EC (NT MDT) equipment.

III. RESULTS AND DISCUSSION

A. Structural studies

Figures 1(a) and (b) show the microstructure of two different places on the surface of the Pr-Fe-Ti-Al-Cu-B magnet with 3 wt.% HoH_2. The nonuniform composition of the 2-14-1-phase grains is visualized in subplot (a), and the cores of the grains are marked by circles. Digits in subplot (b) denote the points where the electron microprobe analysis (EMA) was carried out. According to the XRD and EMA data, four structural components were found (Table I). The main magnetic phase $(Pr,Ho)_2Fe_{14}B$-based (2-14-1) is depleted of rare-earth metals (REMs) because the (Pr+Ho+Nd) content corresponds to only 32 wt.% and Nd is present as an impurity in the starting Pr. It is a tetragonal $Nd_2Fe_{14}B$-type phase with space group $P4_2/mnm$. Phase 2 appears as $(Pr,Ho)_{rich}$, with a relatively high amount of Cu that was found mainly at the ternary junctions of 2-14-1 grains. Finally, phases 3 and 4 are Ti-based and $(Pr, Ho)_2O_3$ oxide phases, respectively.

Since the Ho-containing powder is introduced from the grain boundaries, the distributions of Ho in the 2-14-1 phase grains and the grain boundaries of the final magnet are critical for coercivity enhancement. The Ho distribution within the main magnetic phase grains was studied in detail and is shown in Figures 1(c–g). We found that Ho was distributed nonuniformly, that is, the cores of grains were Ho-depleted, whereas their edges were Ho-enriched. Therefore, we could observe typical "core-shell" structure formation (Fig. 1a) when HoH_2 hydride additions were used in the powder mixture.

Powders at different stages of the preparation process were studied by XRD to determine precisely the lattice parameters of the main magnetic phase (Table II). The base alloy (wt.%) Pr-33, Ti-0.9, Al-0.3, Cu-0.15, B-1.3, Fe-balance, which was first subjected to hydrogen decrepitation, and its mixture with 3 wt.% HoH_2 were subjected to dehydrogenation during heating at 775 K for 1 h in a vacuum of 1.33×10^{-2} Pa. The results show that (i) the lattice parameters of the alloy prepared with holmium hydride are slightly higher

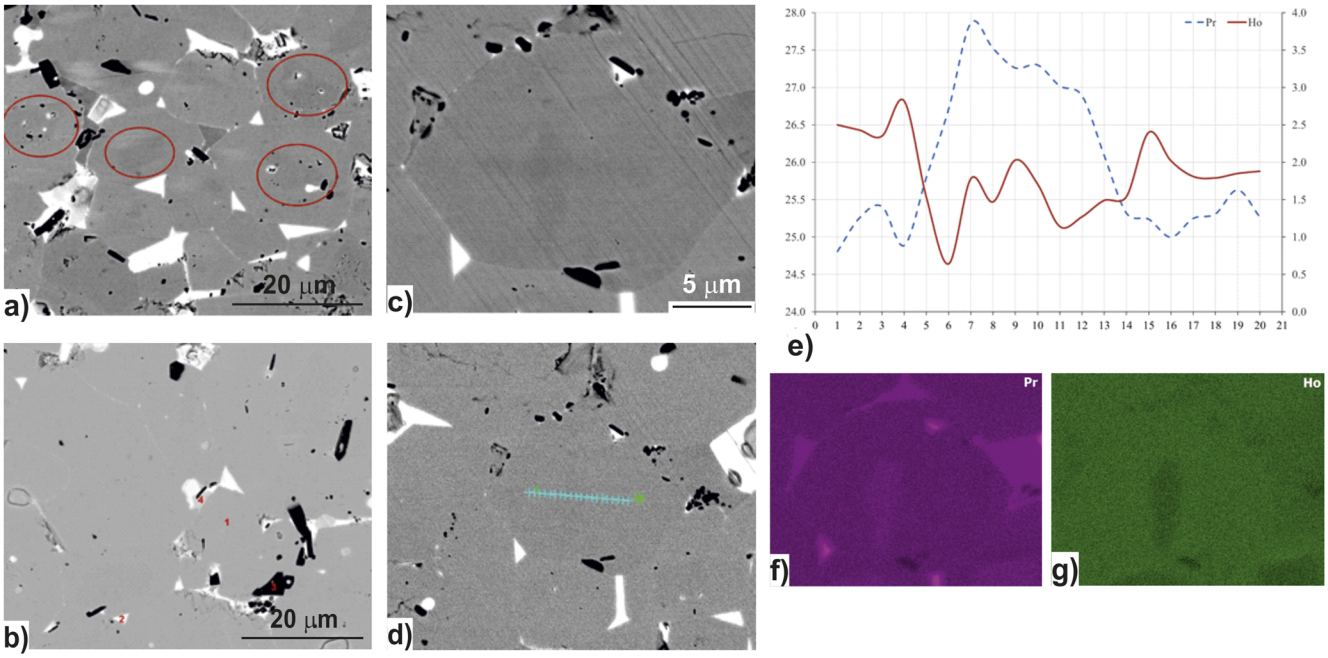

FIG. 1. (a, b) Scanning electron microscopy (SEM) images of the (Pr, Ho)$_2$Fe$_{14}$B-based magnet obtained from two different points on the surface in the back-scattering electron (BSE) mode; (a) circles indicate the cores of grains; (b) digits correspond to electron microprobe analysis (EMA) points (Table I). (c, d) Amplified SEM images of 2-14-1 phase grain; (e) EMA data along the scanning line highlighted in subplot (d); (f) Pr distribution map; (g) Ho distribution map.

than those of the Ho-free alloy indicating the introduction of Ho into the 2-14-1 lattice rather than the substitution of Ho for Nd and (ii) the lattice parameters a and c of dehydrogenated alloys decreased in agreement with literature data[12] indicating the compensation of hydrogen in the lattice on dehydration at the expense of HoH$_x$ or the transition of hydrogen into 2-14-1 from the hydride.

TABLE I. Electron microprobe analysis (EMA) data (wt.%) of the (Pr,Ho)-Fe-B magnet.

Element/phase	O	Al	Ti	Pr	Nd	Fe	Ho	Cu
Area_mean	3.1	0.6	1.3	30.1	1.5	57.1	4.6	0.6
Phase_1_mean	1.6	0.5	0.3	24.5	1.3	64.8	5.2	0.6
Phase_2_1[a]	2.6	0.4	0.2	80.7	2.0	4.3	0.3	8.4
Phase_2_2	1.9	0.4	0.4	78.3	2.5	4.7	1.9	8.8
Phase_2_3	2.0	0.4	1.1	71.9	2.2	11.1	1.5	8.4
Phase_2_4	2.4	0.5	0.3	78.4	2.6	4.5	1.4	8.5
Phase_2_5	2.2	0.4	0.2	78.7	2.2	6.3	0.7	8.3
Phase_2_6	2.0	0.4	0.4	72.9	2.6	11.5	1.2	7.9
Phase_3_1*	1.5	0.1	76.1	11.9	0.6	7.4	1.1	0.8
Phase_3_2	1.1	0.2	70.9	10.5	0.4	13.1	1.5	1.2
Phase_3_3	1.4	0.5	45.1	16.5	0.9	31.8	2.5	0.5
Phase_4	16.4	0.1	0.4	71.0	2.6	6.5	2.3	0.3

[a]Compositions of the (Pr, Ho)$_{rich}$ and (Pr, Ho)$_2$O$_3$ oxide phases vary.

B. Magnetic measurements

Figures 2(a) and (b) show the magnetization reversals of the (Pr,Ho)-Fe-B permanent magnets measured at different temperatures. It can be seen that the values of the magnetic parameters obtained from the hysteresis loops of the Ho-enriched sample are substantially higher than those of Pr-Fe-B (see Table III), despite the fact that Ho atoms are antiferromagnetically ordered with respect to Fe atoms.[13] Measurements performed at low temperatures indicate the progressive increase in the values of the magnetic induction and the maximum energy product (Table IV). Due to slow increase of B_r with decreasing temperature (inset of Figure 2(a)), we can state that no SRT takes place at temperatures down to 4.2 K.

It might seem that an improvement in the magnetic properties of the Ho-rich magnet could be related to the presence of Ho in the Pr$_2$Fe$_{14}$B crystal lattice and the formation of the "core-shell" structure of the phase grains. It is known that the alloying of Nd$_2$Fe$_{14}$B-based magnets with Dy and Tb leads to an increase in the coercive force and is related to the higher anisotropic fields of the Dy$_2$Fe$_{14}$B and Tb$_2$Fe$_{14}$B compounds.[7] An analogous explanation can be given for alloying with Ho since the anisotropic field of Ho$_2$Fe$_{14}$B is slightly higher than that of Nd$_2$Fe$_{14}$B,[11] but almost identical to or slightly lower than that of Pr$_2$Fe$_{14}$B,[7] and cannot be responsible for such a marked increase in the coercive force of (Pr,Ho)-Fe-B magnets. Our explanation is based on the conclusions reached in the literature,[14,15] which are that alloying of the Nd$_2$Fe$_{14}$B structure with heavy REMs (Dy and Tb) results in its stabilization, in

TABLE II. Variations in the lattice parameters of the main magnetic phase $(Pr,Ho)_2Fe_{14}B$ following hydrogenation and dehydrogenation in the course of preparation of the magnets.

Powder state	a (nm)	c (nm)	$a^2 \times c$ (nm^3)	ΔV (nm^3)
$Pr_2Fe_{14}BH_x$	0.8873(6)	1.2352(14)	$V_1 = 0.97261$	$\Delta(V_1 - V_3) = 24.71$
$Pr_2Fe_{14}BH_x + HoH_2$	0.8877(6)	1.2354(16)	$V_2 = 0.97351$	$\Delta(V_2 - V_1) = 0.90$
Dehydrogenated $Pr_2Fe_{14}BH_x$	0.8793(8)	1.226(3)	$V_3 = 0.94790$	$\Delta(V_2 - V_4) = 23.32$
Dehydrogenated $Pr_2Fe_{14}BH_x + HoH_2$	0.8798(7)	1.227(3)	$V_4 = 0.95019$	$\Delta(V_4 - V_3) = 2.29$

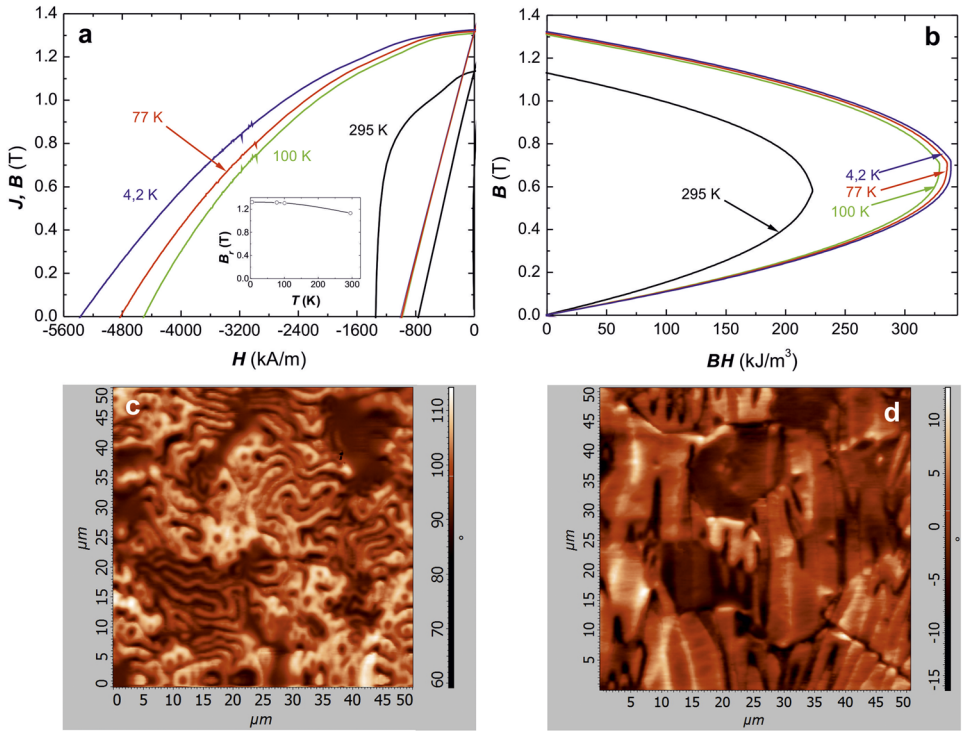

FIG. 2. (a, b) Magnetic properties of the (Pr, Ho)-Fe-B magnet measured using the VSM: (a) *J–H* and *B–H* dependences (plotted with allowance for the demagnetizing factor) measured at different temperatures; (inset) dependence of B_r on temperature *T*; (b) maximum energy product $(BH)_{max}$. (c, d) Magnetic force microscopy (MFM) data obtained from the (Pr, Ho)-Fe-B magnet in directions (c) perpendicular (pole surface) and (d) parallel (lateral surface) to the magnetic texture.

contrast to the effect of light REMs (La, Pr). Similarly, we can assume that Ho, as a heavy REM, also stabilizes the $Nd_2Fe_{14}B$-type structure and favors the higher resistance to the formation of crystal lattice stacking defects. The importance of the role of the structural state of the main magnetic field was discussed by our group in Reference 16.

TABLE III. Room temperature bulk magnetic parameters of Pr-Fe-B and (Pr, Ho)-Fe-B magnets obtained from the measured hysteresis loops; B_r – remanence of the magnetic flux density; ${}_jH_c$ – coercivity of the magnetic polarization (*J–H* curve); ${}_jH_b$ – coercivity corresponding to the *B–H* curve; H_k – parameter adopted as a criterion of coercivity (i.e., the magnetic field determined at $0.9 \times B_r$); $(BH)_{max}$ – maximum energy product.

Sample	B_r (T)	${}_jH_c$ (kA/m)	${}_bH_c$ (kA/m)	H_k (kA/m)	$(BH)_{max}$ (kJ/m^3)
Pr-Fe-B	1.09	1404	702	335	191
(Pr, Ho)-Fe-B	1.11	1516	806	893	223

Figures 2(c) and (d) show the domain structure of the (Pr, Ho)-Fe-B magnet studied by magnetic force microscopy (MFM). Typical labyrinth magnetic domains were observed on the pole surfaces of the magnet, while the lateral surfaces demonstrated strip domains, which were observed in almost all 2-14-1-phase grains.

TABLE IV. Magnetic parameters of (Pr, Ho)-Fe-B magnet as a function of the applied temperature. Due to limited space in the oven, small magnet pieces were measured using the vibrating-sample magnetometer.

T (K)	B_r (T)	${}_jH_c$ (kA/m)	${}_bH_c$ (kA/m)	$(BH)_{max}$ (kJ/m^3)
295	1.13	1344	764	221
100	1.31	4527	971	327
77	1.32	4837	987	332
4.2	1.33	5402	1011	336

Such a domain-structure pattern indicates the adequate magnetic texture of the magnet, which was formed during texturing of the Ho-containing Pr-Fe-B powder in the magnetic field. The average domain width was 1.2–1.8 μm.

IV. CONCLUSIONS

We draw the following main conclusions from a careful analysis of the results of our study.

(1) Sintered permanent Pr-Ho-Fe-Ti-Al-Cu-B magnets were prepared using HoH_2 additions, and the following magnetic characteristics were obtained at room temperature: B_r = 1.13 T; ${}_jH_c$ = 1344 kA/m; $(BH)_{max}$ = 221 kJ/m^3. Marked improvements in the magnetic properties were achieved by cooling the magnet to 77 K and 4.2 K: B_r = 1.32 T; ${}_jH_c$ = 4837 kA/m; $(BH)_{max}$ = 332 kJ/m^3 and B_r = 1.33 T; ${}_jH_c$ = 5402 kA/m; $(BH)_{max}$ = 336 kJ/m^3.

(2) The dependence of the B_r on the temperature exhibits no spin reorientation down to 4.2 K.

(3) The phase composition of the magnet is characterized by the presence of four structural components: the main magnetic $(Pr,Ho)_2Fe_{14}B$, $(Pr,Ho)_{rich}$, $(Pr,Ho)_2O_3$ oxide, and Ti-based phases. The Ho content in the $(Pr,Ho)_{rich}$ phase was found to be lower than that in the main magnetic 2-14-1 phase.

ACKNOWLEDGMENTS

This paper was created within the project LTARF18031 "Development of physico-chemical and engineering foundations for the initiation of innovative resources-economy technology of high-power and high-coercivity (Nd,R)-Fe-B (R = Pr, Tb, Dy, Ho) low-REM permanent magnets" and within Project No. 14.616.21.0093 (unique identification number RFMEFI61618X0093). The studies were carried out using the research infrastructure of the Regional Materials Science and Technology Centre, VSB-Technical University of Ostrava (Czech Republic) and the Centre of Collaborative Access for Functional Nanomaterials and High-Purity Substances, Baikov Institute of Metallurgy and Materials Science, Russian Academy of Sciences.

REFERENCES

[1] F.-J. Borgermann, C. Brombacher, and K. Uestuener, Proceedings of IPAC **2014**, 1238.
[2] K. Skotnicova, G. S. Burkhanov, Yu. S. Koshkid`ko, D. Růžička, T. Cegan, J. Cwik, N. B. Kolchugina, A. A. Lukin, O. Zivotsky, and K. Hrabovská, Metalurgija **55**, 621 (2016).
[3] C. Benabderrahmane, M. Valléau, P. Berteaud, K. Tavakoli, J. L. Marlats, R. Nagaoka, N. Béchu, D. Zerbib, P. Brunelle, L. Chapuis, D. Dallé, C. Herbeaux, A. Lestrade, M. Louvet, and M. E. Couprie, J. Phys.: Conf. Ser. **425**, 032019 (2013).
[4] S. Hirosawa, Y. Matsuura, H. Yamamoto, S. Fujimura, M. Sagawa, and H. Yamauchi, J. Appl. Phys. **59**, 873 (1986).
[5] K. H. J. Buschow, Mater. Sci. Rep. **1**, 1 (1986).
[6] E. P. Wohlfarth and K. H. J. Buschow, (Eds.), in *Ferromagnetic Materials*, Vol. 4, North-Holland, Amsterdam, 1988.
[7] E. B. Boltich and W. E. Wallase, Solid State Commun. **55**, 529 (1985).
[8] Y. B. Kim, M. J. Kim, and J. Han-Min, J. Magn. Magn. Mater. **191**, 133 (1999).
[9] B. Chen, X. Liu, R. Chen, S. Guo, D. Lee, and A. Yan, J. Alloys Comp. **516**, 73 (2012).
[10] C. H. Lin, C. J. Chen, T. Y. Liu, W. C. Chang, and C. D. Wu, J. Appl. Phys. **69**, 5518 (1991).
[11] L. Liang, T. Ma, C. Wu, P. Zhang, X. Liu, and M. Yan, J. Magn. Magn. Mater. **397**, 139 (2016).
[12] S. Obbade, S. Miraglia, P. Wolfers, J. L. Soubeyroux, D. Fruchart, F. Lera, C. Rillo, B. Malaman, and G. le Caer, J. Less-Common Met. **171**, 71 (1991).
[13] M. J. Cooper, E. D. N. Timms, R. Armstrong, F. Itoh, Y. Tanaka, M. Ito, H. Kawata, and R. Bateson,. Phys. Rev. Lett. **71**, 1095 (1993).
[14] X. B. Liu and Z. Altounian, J. Appl. Phys. **111**, 07A701 (2012).
[15] X. B. Liu, Z. Altounian, M. Huang, Q. Zhang, and J. P. Liu, J. Alloys Comp. **549**, 366 (2013).
[16] A. A. Lukin, N. B. Kolchugina, G. S. Burkhanov, N. E. Klyueva, and K. Skotnicova, Inorg. Mater. Appl. Res. **4**, 256 (2013).